Testing the Steric Exclusion Model for Hexameric Helicases: Substrate Features That Alter RNA−DNA Unwinding by the Transcription Termination Factor Rho†

Céline Walmacq,‡,§ A. Rachid Rahmouni,‡ and Marc Boudvillain*,‡

Centre de Biophysique Moléculaire (UPR4301), CNRS, rue Charles Sadron, 45071 Orléans Cedex 2, France, and Ecole doctorale Sciences et Technologies, Université d'Orléans, France

Received January 12, 2006; Revised Manuscript Received March 3, 2006

ABSTRACT: Typical hexameric helicases form ring-shaped structures involved in DNA replication. These enzymes have been proposed to melt forked DNA substrates by binding to, and pulling, one strand within their central channel, while the other strand is forced outside of the hexamer by steric exclusion and specific contacts with the outer ring surface. Transcription termination factor Rho also assembles into ring-shaped hexamers that are capable to use NTP-derived energy to unwind RNA and RNA−DNA helices. To delineate the potential relationship between helicase structural organization and unwinding mechanism, we have performed in vitro Rho helicase experiments with model substrates containing an RNA−DNA helix downstream from a Rho loading site. We show that a physical discontinuity (nick) inhibits RNA−DNA unwinding when present in the RNA but not in the DNA strand. Moreover, the presence of a 3′-overhanging DNA tail (Y-shaped substrate) does not affect initial Rho binding but can impair helicase activity. This inhibitory effect varies with the length of the tail, is independent of the identity (A or U) of the tail residues, and is also obtained when a biotin−streptavidin complex replaces the single-stranded DNA arm. However, it is readily relaxed upon moving the reporter RNA−DNA helix farther from the Rho loading site. The data indicate that the Rho helicase uses a steric exclusion mechanism whereby the initial formation of a productive Rho−transcript complex is a crucial rate-limiting event, while no specific interactions with the displaced strand are required. These results outline significant similarities as well as some differences in the mechanism of unwinding between Rho and other hexameric helicases which are discussed in relation with the biological function of the Rho helicase.

Transcription termination factor Rho mediates the release of the nascent transcript from the ternary transcription elongation complex (TEC)[1] at specific sites along the DNA template (*1*, *2*). The functional form of the Rho protein is a homo-hexamer which has a quaternary structure similar to the ones of ring-shaped hexameric helicases involved in DNA replication (*3*). Some functional analogies are also evident since the Rho factor possesses in vitro RNA-dependent NTPase (*4*) and NTP-dependent RNA and RNA−DNA helicase (*5*, *6*) activities. Notably, Rho can dissociate a nucleic acid (NA) strand provided that it is hybridized downstream from an appropriate 'loading site' along the RNA chain (*5*−*9*). The presence of such loading sites, termed *Rut* (for *R*ho *Ut*ilization) sites, on the nascent transcript is also necessary for Rho to induce termination of transcription (*10*−*13*). The *Rut* sites are usually 60−80 nucleotides (nt)-long sequences enriched in C-residues, poor in G-residues, and exhibiting little secondary structure content. Although no more precise consensus could be clearly defined for the *Rut* sites (*14*−*18*), synthetic polypyrimidine repeat sequences (>40 nt) can make efficient artificial loading sites (*aRut* sites) for Rho-dependent termination of transcription (*19*) and Rho helicase activity (*7*). The *Rut* (and, presumably, *aRut*) sequences contact and circle on the primary binding site that crowns the surface of the Rho hexamer (*20*, *21*). This interaction, together with the marked helical twist of open Rho conformers, is thought to drive the downstream transcript section within the central hole of the hexamer ring (*21*, *22*). There, RNA contacts with the Rho secondary RNA binding site could induce closure of the hexamer ring and activate ATP hydrolysis (*21*, *23*−*26*). This, in turn, likely fuels 5′-3′ enzyme tracking along the transcript until Rho catches up with and disrupts the TEC, presumably by using its helicase (translocase) activity (*1*, *2*).

At present, the exact mechanisms used by Rho to dissociate NA and protein roadblocks have not been determined. However, the extensive mechanistic information existing for DNA helicase counterparts (*3*, *27*−*29*) may be used as a guide to design and test models for the Rho helicase. To initiate DNA unwinding in vitro, hexameric DNA helicases usually require two noncomplementary single-stranded DNA (ssDNA) tails flanking a duplex DNA region (Y-shaped substrate; (*3*)). These helicases load onto one of the ssDNA tails and likely use the second tail as a mechanical device to effect duplex unwinding (*30*−*34*). Indeed, in the absence of

† This research was funded in part by the Association pour la Recherche sur le Cancer (Grant No. 3639), the Ligue contre le Cancer (Région Centre), and Biotechnocentre.

* Corresponding author. Phone, +33 238 25 55 85; fax, +33 238 63 15 17; e-mail, boudvill@cnrs-orleans.fr.

‡ Centre de Biophysique Moléculaire (UPR4301), CNRS.

§ Université d'Orléans.

[1] Abbreviations: NA, nucleic acid; TEC, transcription elongation complex; PAGE, polyacrylamide gel electrophoresis.

10.1021/bi0600648 CCC: $33.50
Published on Web 04/08/2006

this second ssDNA tail, prototypical DnaB and Mcm helicases do not unwind the duplex region but rather engulf the two DNA strands into their central channels (*32*−*34*). Conversely, the bulk of a streptavidin−biotin complex in place of the second ssDNA tail is sometimes sufficient to trigger duplex unwinding (*31*, *33*). From these data, it has been proposed that ring-shaped DNA helicases operate through a DNA steric exclusion mechanism whereby one strand of the DNA substrate is pulled in the central channel of the hexamer, while the other strand is excluded from the center of the ring during unwinding (*3*, *30*−*36*). 'In-register' outer helicase contacts with the excluded DNA strand could also facilitate duplex unwinding (*30*, *35*, *36*). Despite obvious differences between Rho and hexameric DNA helicases (biological function, NA substrate, primary interaction subsite, nature of the roadblock target), common features (ring shape, substrate path within a central channel of comparable dimensions) suggest that a steric exclusion model could also provide the mechanistic basis for Rho-dependent termination of transcription (*37*). Here, we have used in vitro helicase experiments with model NA substrates to explore this possibility. We show that Rho hexamers can remove various kinds of NA and nucleoproteic roadblocks located along an RNA molecule. Moreover, Rho disruption of intervening obstacles appears to proceed through a mechanism that exhibits many similarities with the steric-exclusion mechanism proposed for other hexameric helicases. Yet, Rho also presents specific responses to some molecular features of its NA (or nucleoproteic) substrate that point to subtle mechanistic differences with its DNA helicase counterparts and that identify spatial remodeling of the Rho−substrate complex early on the reaction pathway as a crucial rate-limiting step.

MATERIALS AND METHODS

Materials. Chemicals and enzymes were obtained from Sigma-Aldrich and New England Biolabs, respectively. Oligonucleotides were purchased from Distribio (France) and were systematically purified by polyacrylamide gel electrophoresis (PAGE). The Rho protein (concentrations expressed in units of hexamers throughout the manuscript) and poly(rC) fragments (>300 nt) were prepared and characterized as described previously (*7*, *38*).

The pCW05 and pAS02 plasmids were obtained by inserting double-stranded oligonucleotides containing the T7 promoter and *aRut* sequences between, respectively, the *Hpa*I and *Sma*I or *Hpa*I and *Acc65*I sites of plasmid pSP73 (Promega). The DNA templates encoding the various transcripts (the RNA sequences are shown in the figures) were prepared by linearization of pAS02 with *Sma*I (R_{157} transcript) or by PCR amplification of specific regions of the pCW05 (R_{103} transcript) and pAS02 (R_{43} and R_{115} transcripts) plasmids. The in vitro transcriptions of these templates with T7 RNA polymerase were performed as described previously (*39*) using larger reaction volumes (500 μL) and longer incubation times (2−3 h). The transcripts were purified by 7% denaturing PAGE and stored at −20 °C in $M_{10}E_1$ buffer (10 mM MOPS, pH 6.5, and 1 mM EDTA).

Preparation of the RNA−DNA Constructs. Typically, 10 pmol of ^{32}P-labeled oligonucleotides were mixed with 1.1 molar equivalents of transcripts in 20 μL of hybridization buffer (150 mM potassium acetate {AcK}, 20 mM HEPES, pH 7.5, and 0.1 mM EDTA) and heated for 2 min at 95 °C. The mixtures were slowly cooled to room temperature over 60 min before being mixed with 5 μL of loading buffer (15% [w/v] Ficoll-400 and 0.1 M EDTA). The RNA−DNA constructs were then purified from the reaction mixture by 6−8% nondenaturing PAGE and stored at −20 °C in helicase buffer (*7*). The NA concentrations were determined by UV measurements with a microliter-spectrophotometer (Nanodrop) and/or from specific activities of the samples. The Mfold software (*40*) and nearest-neighbor calculations (*41*) were used to predict, respectively, the secondary structures of the constructs and stabilities of the RNA−DNA helices.

Helicase Assays. Helicase assays were performed as described previously (*7*). Briefly, the RNA−DNA constructs (0.15 pmol) were mixed with a 4-fold molar excess of Rho hexamers in 27 μL of helicase buffer (hybridization buffer supplemented with 0.5 mM DTT) and incubated for 3 min at 30 °C. Then, the helicase reaction was initiated with 3 μL of a solution containing ATP, $MgCl_2$ (1 mM, final concentrations), and DNA traps (13.5 pmol of unlabeled oligonucleotides identical to the ones annealed to the transcript). For single-turnover experiments, an excess of poly rC (3 μM in rC residues) was also included in the initiation mix. Reaction aliquots were taken at various times, mixed with 4 vol of quench buffer (180 mM AcK, 25 mM EDTA, 0.625% SDS, and 3.75% Ficoll-400), and resolved by nondenaturing PAGE (gels contained 0.5% SDS). Reactions performed with the forked RNA−DNA substrates were analyzed on 4%:12% (top/bottom) stacked gels, whereas other samples were run on continuous 8 or 10% gels. Helicase experiments were performed at least in triplicate unless otherwise specified. Detection and quantification of gel bands were performed with a Storm-860 Phosphorimager and related software (Molecular Dynamics). The fractions of individual products present in the reaction at a given time were determined with the following formula:

$$F_t = (I_t - F_0 \times \sum I_{i,t})/[(1 - F_0) \times F_\Delta \times \sum I_{i,t}]$$
$$\text{with } F_0 = I_0/\sum I_{i,0} \quad \text{and } F_\Delta = I_\Delta/\sum I_{i,\Delta}$$

where I_0, I_t, and I_Δ are the intensities of the product bands after incubation of the helicase reaction for 0 or *t* minutes at 30 °C or after 2 min at 95 °C, respectively ($\sum I_{i,0}$, $\sum I_{i,t}$, and $\sum I_{i,\Delta}$ are the sums of the intensities of the bands per gel lane measured under the same respective conditions). Note that $F_0 < 0.02$ in most experiments and that $F_\Delta = 1$ for reactions performed with RNA−DNA constructs containing only one ^{32}P-labeled oligonucleotide.

RESULTS

Rho Unwinding Activity Is Differentially Affected by Nicks in the DNA and RNA Strands. To facilitate the quantitative analysis of Rho helicase activity in vitro, we have designed recently synthetic RNA−DNA model substrates (*7*). These constructs were made of a ^{32}P-labeled oligodeoxyribonucleotide annealed to a ~200 nt-long transcript containing a synthetic *aRut* loading site (47 nt). Efficient Rho-directed unwinding of the RNA−DNA hybrids depended on a number of factors such as the presence of a single-stranded *aRut* region within the transcript as well as the location of the

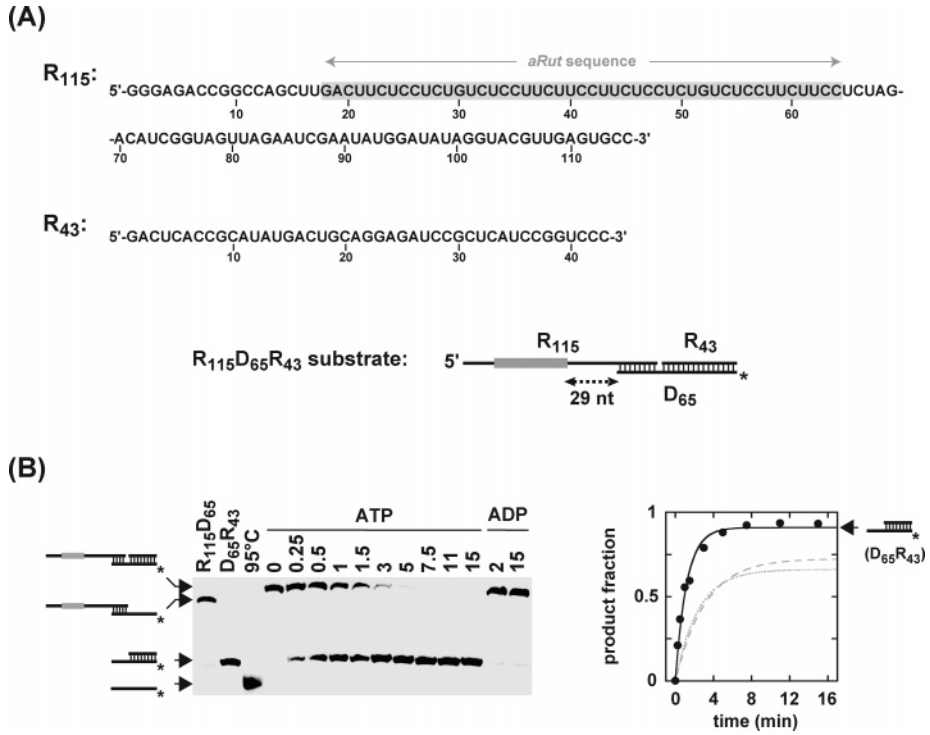

FIGURE 1: Rho-directed unwinding of an RNA−DNA hybrid containing a nick in the RNA strand. **(A)** A schematic of the $R_{115}D_{65}R_{43}$ substrate is shown together with the sequences of its RNA components. Two contiguous RNA−DNA helices (22 and 43 bp) are formed downstream from the *aRut* site (gray box) upon pairing of the D_{65} oligonucleotide with the R_{115} and R_{43} transcripts. The ^{32}P-label on the D65 oligonucleotide is depicted by an asterisk. Control hybrid substrates containing an overhanging ($R_{115}D_{65}$ substrate) or blunt-ended ($R_{115}D_{22}$ substrate) DNA 5′-end were also prepared. **(B)** Representative 10% nondenaturing polyacrylamide gel showing products of the helicase reaction with the $R_{115}D_{65}R_{43}$ substrate. Starting material and potential reaction products are schematically depicted on the left side of the gel. The $R_{115}D_{65}R_{43}$ construct (5 nM) was incubated for 3 min at 30 °C with an excess of Rho hexamers (20 nM) in standard helicase buffer (150 mM AcK, 20 mM HEPES, pH 7.5, 0.1 mM EDTA, and 0.5 mM DTT). The helicase reaction was initiated by the addition of $MgCl_2$ (1 mM), ATP (1 mM), poly(rC) (3 μM in rC residues), and an excess of unlabeled D_{65} oligonucleotide (450 nM, to trap the RNA strands released during the reaction). In control experiments, ATP was replaced by ADP. At various times (indicated in minutes above the gel lanes), aliquots were removed from the helicase mixtures, mixed with quench buffer, and loaded on a gel containing 0.5% SDS to denature Rho−NA complexes (*7*). Samples of the $R_{115}D_{65}$ and $D_{65}R_{43}$ hybrids as well as a reaction aliquot that was heated at 95 °C were also loaded on the gel. The graph shows the fraction of ^{32}P-labeled $D_{65}R_{43}$ product released from the R_{115} transcript as a function of time (black continuous line and filled circles). A fit of the data to an equation describing pseudo-first-order $D_{65}R_{43}$ progress yielded the following reaction amplitude and observed rate constant: $A = (0.9 \pm 0.02)$ and $k_{obs} = (0.85 \pm 0.07)$ min^{-1}. Progress curves corresponding to DNA oligonucleotides displaced by Rho from the control $R_{115}D_{65}$ (long-dashed line) and $R_{115}D_{22}$ (dotted line) constructs are also shown for comparison.

RNA−DNA helix sufficiently far (≥18 nt) downstream from the *aRut* sequence (*7*). Moreover, the fraction of oligonucleotides released during one helicase round decreased when the length of the RNA−DNA helix increased. In agreement with previous work (*5*, *8*, *9*, *42*, *43*), the data suggested that the Rho helicase uses a single-stranded region encompassing the *aRut* site to load productively onto the transcript and then move directionally along the RNA chain using NTP hydrolysis as the energy source. The fact that Rho directional translocation could trigger unwinding of the RNA−DNA hybrid in a succession of identical and moderately processive discrete steps has also been proposed (*7*). However, important features of Rho translocation and helicase activities, such as the nature of the rate-limiting step, the size of the translocation step, or the transient molecular contacts made with the substrate during unwinding, could not be unveiled in these studies.

To comprehend the molecular specifics of Rho-directed NA unwinding in greater detail, we have prepared and probed synthetic RNA−DNA variants bearing various molecular modifications. First, we assessed the effect of strand nicks introduced within the hybrid region on the activity of the Rho helicase. To this end, the $R_{115}D_{65}R_{43}$ substrate was assembled from separate DNA and RNA components (Figure 1A) and purified by native PAGE. This composite substrate contains a 65 base pair-(bp)-long RNA−DNA region located 29 nt downstream from the 3′-end of the *aRut* site (Figure 1A). Moreover, the hybrid region is interrupted by a nick in the RNA strand and is therefore made of two contiguous RNA−DNA helices, and the shorter one (22 bp, $\Delta G_{hyb} = -27.8$ kcal/mol) is in front of the longer helix ($\Delta G_{hyb} = -63.8$ kcal/mol; note that potential energetic contributions arising from mutual helix stacking are not accounted for by ΔG_{hyb} values; see ref *44*). In this way, disruption of the downstream helix is likely to require direct helicase action rather than to result from indirect destabilization (due, for instance, to the propagation of steric constraints arising during unwinding of the upstream helix). The $R_{115}D_{65}R_{43}$ hybrid substrate (5 nM) was incubated in standard helicase buffer for 3 min at 30 °C with an excess of Rho hexamers before addition of a mix containing equimolar amounts of $MgCl_2$ and ATP as well as NA traps (single-run conditions; see methods and refs *7* and *8*). At various times, aliquots were removed from the reaction mixture and analyzed by PAGE. As shown in Figure 1B, the Rho helicase effectively disrupted the upstream helix of the $R_{115}D_{65}R_{43}$ substrate

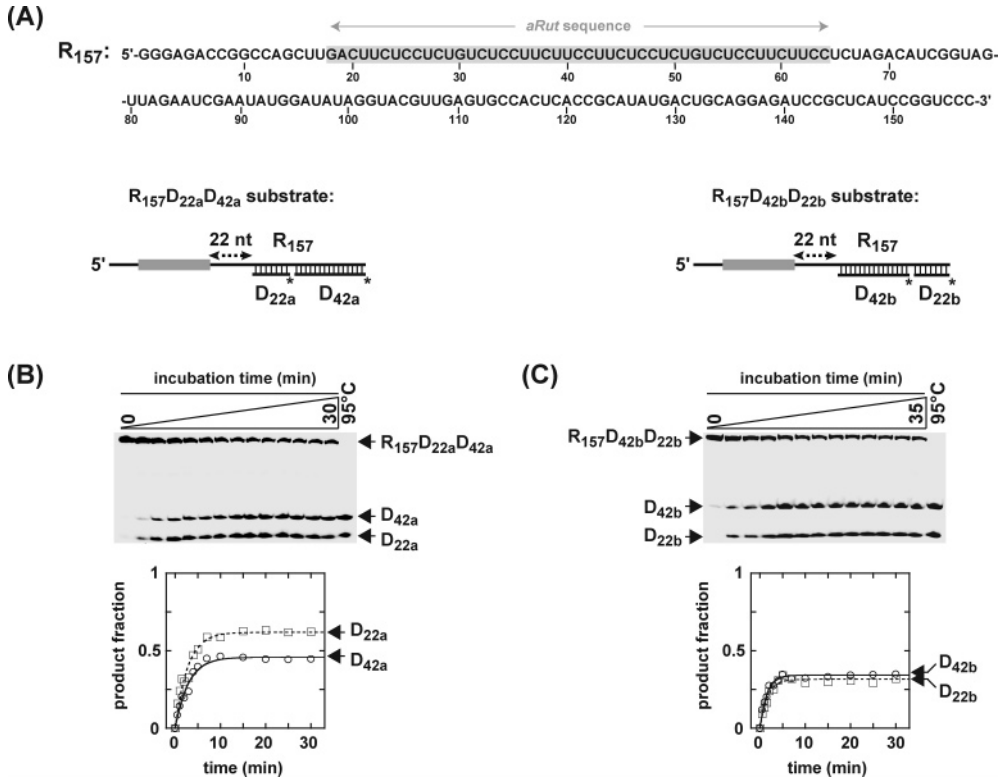

FIGURE 2: Unwinding of RNA−DNA constructs containing a nick in the DNA strand. **(**A**)** The sequence of the R_{157} transcript is shown together with schematics of the RNA−DNA constructs. In the $R_{157}D_{22a}D_{42a}$ substrate, a short RNA−DNA helix (22 bp, $\Delta G_{hyb} = -27.8$ kcal/mol) precedes a contiguous 42 bp-long hybrid region ($\Delta G_{hyb} = -62.5$ kcal/mol), whereas in $R_{157}D_{42b}D_{22b}$, the 42 bp-long helix ($\Delta G_{hyb} = -57.1$ kcal/mol) is located in front of the shorter hybrid (22 bp, $\Delta G_{hyb} = -32.3$ kcal/mol). The ^{32}P-labels are depicted by asterisks. Representative 10% polyacrylamide gels show the evolution of NA species during helicase reactions with the $R_{157}D_{22a}D_{42a}$ **(**B**)** or $R_{157}D_{42b}D_{22b}$ **(**C**)** substrate. Experiments were performed as described in the legend to Figure 1. The fractions of ^{32}P-labeled oligonucleotides released as a function of time were determined as described in Materials and Methods and were averaged from three independent experiments. Nonlinear least-squares fits of the data yielded: $A = (0.62 \pm 0.02)$ and $k_{obs} = (0.36 \pm 0.05)$ min^{-1} for the release of the D_{22a} strand; $A = (0.45 \pm 0.02)$ and $k_{obs} = (0.38 \pm 0.05)$ min^{-1} for the D_{42a} strand; $A = (0.37 \pm 0.02)$ and $k_{obs} = (0.67 \pm 0.11)$ min^{-1} for the D_{42b} strand; and $A = (0.34 \pm 0.02)$ and $k_{obs} = (0.58 \pm 0.07)$ min^{-1} for the D_{22b} strand.

($D_{65}R_{43}$ product). Moreover, this reaction was more efficient ($k_{obs} = 0.85$ min^{-1} and $A = 0.91$; i.e., 91% of product is formed in one helicase run) than previously observed for unwinding of RNA−DNA helices of comparable lengths ($k_{obs} = 0.3-0.5$ min^{-1}; $A = 0.6-0.7$; see ref *7*). This difference was not due to unsought effects of the Rho trap (poly(rC); see ref *7*) since similar reaction parameters were found for the first helicase run of multiple-cycle experiments performed with $R_{115}D_{65}R_{43}$ (data not shown). On the other hand, Rho disrupted the control bipartite $R_{115}D_{65}$ (containing a 43 nt-long 5′-overhanging ssDNA tail) and $R_{115}D_{22}$ (same hybrid region but without ssDNA tail) substrates with more 'classical' efficiencies ($A \sim 0.7$; $k_{obs} \sim 0.35$ min^{-1}; graph in Figure 1B and data not shown). These data indicate that the presence of the downstream RNA−DNA helix within the $R_{115}D_{65}R_{43}$ substrate facilitates Rho-directed unwinding of the upstream hybrid region. Another important feature of the helicase reaction performed with the $R_{115}D_{65}R_{43}$ construct is the absence of unwinding of the downstream $D_{65}R_{43}$ helix (there is no single-stranded D_{65} product formed; Figure 1B). This result could be explained in several ways that are not necessarily mutually exclusive: (1) The nick in the RNA strand could neutralize the Rho helicase simply by insulating the downstream RNA segment from the propagation of critical physical constraints imposed upon the RNA chain by the enzyme. (2) Rho interactions with the DNA strand, if any, could be insufficient to hold the $D_{65}R_{43}$ helix once the upstream helix is unwound. (3) The Rho hexamer could be unable to form extensive contacts with the RNA strand ahead from the location where strand separation actually occurs (i.e., the $D_{65}R_{43}$ helix is released before stabilizing interactions between Rho and R_{43} could develop). In any case, the lack of disruption of the downstream $D_{65}R_{43}$ helix indicates that protein contacts to the RNA strand are critical to RNA−DNA unwinding by the Rho helicase. This feature, however, prevents further probing of the elementary Rho translocation step through the introduction of larger physical gaps within the RNA strand (see ref *45*).

To determine whether similar constraints exist for the DNA strand, we prepared two RNA−DNA constructs bearing a nick in the DNA strand at different positions. The composite $R_{157}D_{22a}D_{42a}$ and $R_{157}D_{42b}D_{22b}$ substrates were assembled from the separate R_{157} transcript and two 5′-end-labeled oligonucleotides (Figure 2A) and purified by PAGE before use in unwinding reactions. Helicase experiments were performed under standard single-cycle conditions and analyzed as described above (see also Materials and Methods). In contrast to a nick in the RNA strand, a DNA gap did not preclude Rho from dissociating the two successive RNA−DNA helices (Figure 2B,C and data not shown). Similar results were obtained with the $R_{157}D_{22a}D_{22b}$ substrate in which the two helices are separated by a 20 nt-long segment of single-stranded RNA (data not shown). These data may indicate that a productive complex is secured along the

substrate by Rho interactions with the DNA strand at distances exceeding 20 nt from the actual location of hybrid unwinding (for a complete rationale, see ref *45*). Alternatively, the Rho helicase may bypass DNA gaps simply because the physical continuity of the DNA strand is not critical to the maintenance of a productive enzyme−substrate complex. We favor the latter explanation because long stretches of single-stranded RNA (>80 nt) between the *Rut* loading site and the double-stranded RNA−DNA target do not seem to affect Rho helicase activity significantly (*7*, *8*).

An important feature of the reactions performed with the $R_{157}D_{22a}D_{42a}$, $R_{157}D_{42b}D_{22b}$, and $R_{157}D_{22a}D_{22b}$ substrates is that the removals of the two successive DNA strands occur with pseudo-first-order kinetics, without lag phases in the reaction time-courses, and at the same rate (Figure 2B and data not shown). This observation indicates that the helicase reaction is controlled by a single kinetic step and, therefore, confirms that RNA−DNA unwinding is not rate-limiting the helicase reaction with *aRut*-containing substrates (*7*). Importantly, it also demonstrates that the slow step controlling overall reaction kinetics precedes actual unwinding of the two RNA−DNA helices. This is because kinetic control at a later stage (i.e., during or after RNA−DNA unwinding) would result in distinct numbers and/or kinds of rate-limiting steps for the releases of the two successive DNA strands (see ref *46*).

A Single-Stranded Tail at the 3′-End of the DNA Strand Does Not Strongly Improve the RNA−DNA Helicase Activity of Rho. With the exception of a few archeal and viral specimens, hexameric DNA helicases require Y-shaped DNA substrates to effect duplex unwinding in vitro (*3*). Although the Rho helicase has distinct substrate requirements (*5*, *6*), we wondered whether it would nevertheless exhibit some preference for forked NA structures. We thus prepared *aRut*-containing RNA−DNA constructs bearing a single-stranded $d(T)_n$ (with $0 < n < 30$ nt) extension at the 3′-end of the DNA strand. The constructs were derived from the RNA substrate used in the above experiments (R_{157}; Figure 2A) but contained a single 24 bp-long RNA−DNA helix located 45 nt downstream from the *aRut* loading site ($R_{157}{}^{3'Tn}D_{24}$ substrates). Helicase reactions were carried out with the $R_{157}{}^{3'Tn}D_{24}$ constructs under both single- and multiple-turnover conditions to rule out any unsought effect of the poly(rC) trap (*32*). Multiple experiments performed under these conditions indicate that the reaction parameters (amplitude and rate of the first helicase run) are not significantly affected by the kinetic regimen or the presence of the poly(rC) trap (Figure 3, top graphs). On the other hand, neither the amplitudes nor the rates of the helicase reactions displayed clear-cut dependencies on the length of the ssDNA tails. However, the extent of experimental variability was somewhat higher than usual with these substrates (typically, standard deviations on helicase parameters do not exceed 15%; ref *7*) which could mask more subtle variation trends. To circumvent this problem, we used LOWESS regression analysis (*47*) which outlines the deterministic trends in data variation independently of model assumption. LOWESS fits were generated with smoothing factors ranging from 10% (small data span during polynomial regression; high potential for local random noise in the estimate) to 90% (large data span and less 'local' regression; high potential for bias of the estimate). As shown in Figure 3, the fits for the reaction

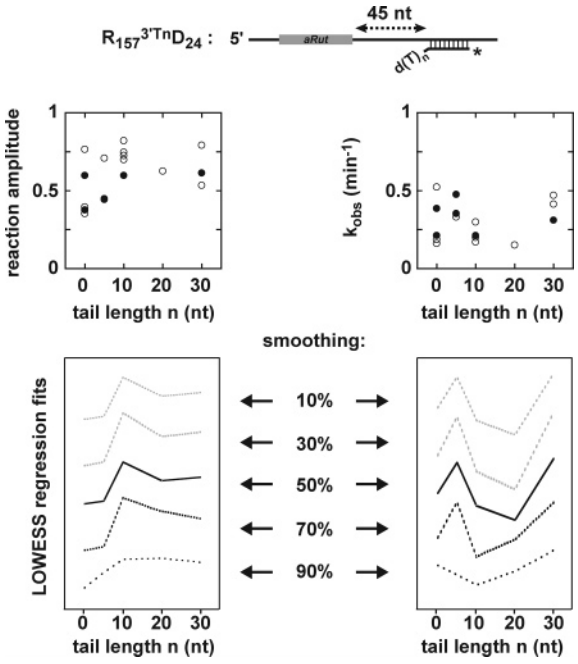

FIGURE 3: Effect of 3′-single-stranded DNA tails on Rho-directed unwinding of the $R_{157}D_{24}$ hybrid substrate. The $^{3'Tn}D_{24}$ oligonucleotides pair with nucleotides 114−137 of the R_{157} transcript ($\Delta G_{hyb} = -33$ kcal/mol) whose sequence is shown in Figure 2. The amplitudes and rates of individual single (black circles)- and multiple (open circles)-cycle experiments are shown on the graphs as a function of the length of the 3′-ssDNA tail. Note that parameters considered for multi-run reactions are the ones of the pre-steady state (exponential) phases. LOWESS regression fits (bottom panels) were determined for various smoothing factors using Kaleidagraph 3.5 (Synergy software).

amplitude (lower left panel) exhibit similar profiles for the complete smoothing range with a small increase in reaction amplitude when the length of the ssDNA tail is increased from 0 to 10 nt and much less variations for longer tails. For the reaction rates, however, the patterns of the fits are more erratic and change for smoothing factors over 50%, suggesting that the experimental variations of k_{obs} with the length of ssDNA tail are essentially random (lower right panel). Altogether, these data indicate that a 3′-ssDNA tail may slightly increase the efficiency of unwinding of the $R_{157}{}^{3'Tn}D_{24}$ substrates by the Rho helicase. This action is much less evident than for replicative DNA helicases, yet it appears to operate in the same direction.

A Bulky Appendage to the 3′-End of the DNA Strand Can Impair Rho Helicase. Due to the uncertainty introduced by the experimental noise observed with the $R_{157}{}^{3'Tn}D_{24}$ substrates (Figure 3), we wanted to corroborate the effect of ssDNA tails on the Rho helicase with another series of RNA−DNA constructs. This series was derived from the minimal $R_{103}D_{24}$ substrate, which contains the same reporter RNA−DNA hybrid than for $R_{157}D_{24}$ but downstream from a 80 nt-long C-rich sequence encompassing the *aRut* motif (Figure 4A). Active disruption of $R_{103}D_{24}$ by the Rho helicase was highly reproducible and about as efficient ($A = [0.63 \pm 0.02]$, $k_{obs} = [0.18 \pm 0.02]$ min^{-1}; Figure 4B, open circles) as for other *aRut*-derived substrates containing RNA−DNA regions of comparable lengths (*7*). Moreover, the presence of a $d(T)_{20}$ extension at the 5′-end of the DNA strand ($R_{103}{}^{5'T20}D_{24}$ substrate) did not affect the helicase reaction (Figure 4B, black circles). On the other hand, the reaction

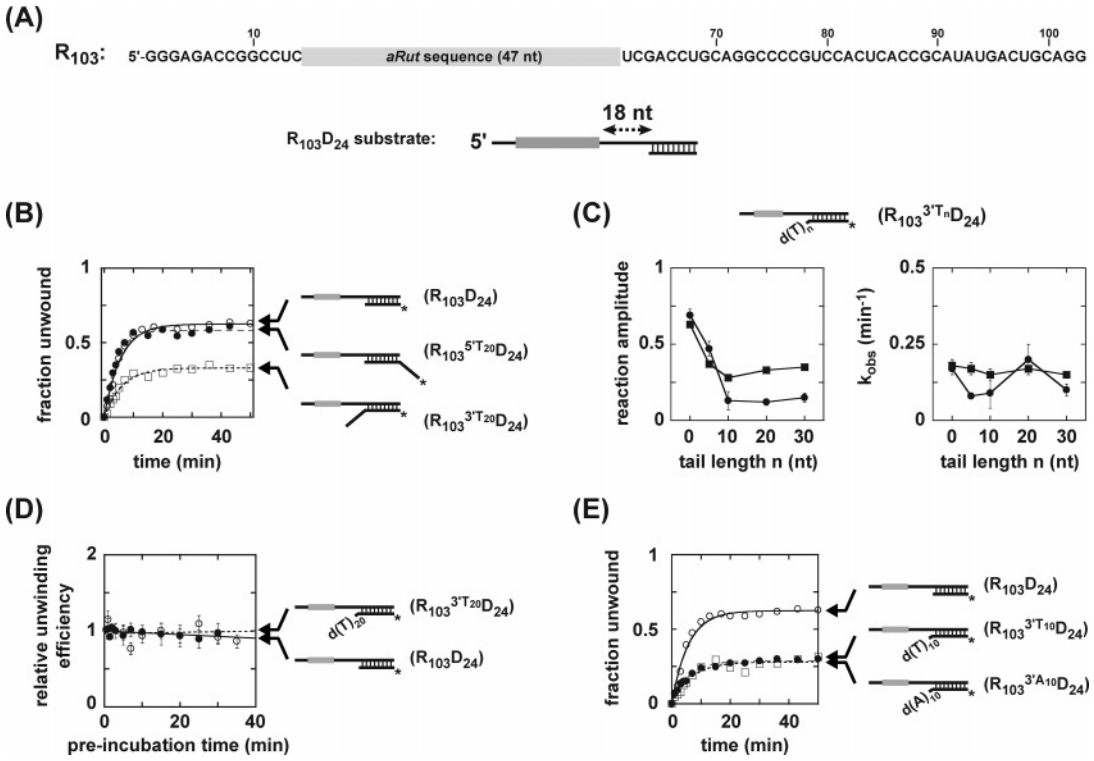

FIGURE 4: Effect of single-stranded sDNA tails on Rho helicase activity with the $R_{103}D_{24}$ substrate derivatives. **(**A**)** Schematic of the parental $R_{103}D_{24}$ substrate which contains a 24 bp-long RNA−DNA helix ($\Delta G_{hyb} = -33$ kcal/mol) at its 3′-end. Minimal single-stranded RNA segments surround the *aRut* site to allow active loading of a unique Rho hexamer onto the substrate and restrict RNA conformational sampling (*7*). **(**B**)** Effect of a single-stranded extension of the DNA strand on the Rho helicase. The $R_{103}{}^{5'T20}D_{24}$ and $R_{103}{}^{3'T20}D_{24}$ substrates contain a $d(T)_{20}$ tail at the 5′- or 3′-end of the hybridized DNA strand, respectively. **(**C**)** Influence of the length of the single-stranded 3′-$d(T)_n$ tail on Rho helicase parameters measured under single (squares)- or multiple (circles)-run conditions. **(**D**)** Unwinding efficiency as a function of the time of preincubation of the Rho−substrate complex before initiation of the helicase reaction with the ATP/Mg^{2+}-containing mix. In each case, the reaction was stopped after 20 min of further incubation at 30 °C. The respective unwinding efficiencies correspond to the fractions of product formed relative to the one obtained under standard conditions (3 min of preincubation). **(**E**)** Single-stranded 3′-$d(T)_{10}$ and 3′-$d(A)_{10}$ extensions of the hybridized D_{24} strand inhibit the Rho helicase to the same extent.

was significantly impaired with the Y-shaped $R_{103}{}^{3'T20}D_{24}$ substrate, wherein the $d(T)_{20}$ extension is situated on the other (upstream) side of the RNA−DNA hybrid (Figure 4B, open squares). This inhibition contradicts the facilitating effect of a 3′-ssDNA tail that was inferred from the results with the $R_{157}{}^{3'Tn}D_{24}$ substrates (see above). To comprehend this discrepancy, helicase experiments were repeated under both single- and multiple-turnover conditions with the complete set of $R_{103}{}^{3'Tn}D_{24}$ substrates ($0 < n < 30$ nt). As shown in Figure 4C, the fraction of hybrid unwound diminished when the length of the 3′-ssDNA tail was increased up to 10 nt and then remained constant for longer $d(T)_n$ extensions. In contrast, the rate of the helicase reaction was hardly affected by the presence of a 3′-ssDNA tail (Figure 4C). These results were, in first approximation, independent of the reaction regimen (Figure 4C) which rules out unwanted trap effects (note that extracting reaction parameters from multi-run progress curves is inherently less precise than for single-run experiments). Furthermore, they indicate that a fork-like structure in front of the RNA−DNA hybrid can partially protect the substrate from effective unwinding, a feature that seemingly demarcates the Rho enzyme from hexameric DNA helicases (see above). Equilibrium binding measurements show that this protection does not stem from interference of the ssDNA tail with the formation of the Rho-substrate complex (Table 1). This was confirmed by preincubation experiments in which unwinding of the $R_{103}{}^{3'T20}D_{24}$ substrate was not affected by the duration of the preincubation with

Table 1: Interaction between Rho Hexamers and *aRut*-Containing Substrates[a]

substrate	F_{max}	n	K_d (nM)	ΔG (kcal/mol)
$R_{103}D_{24}$	0.58 ± 0.06	1.05 ± 0.09	0.61 ± 0.05	−12.8
$R_{103}{}^{3'}T5D_{24}$	0.57 ± 0.08	1.23 ± 0.05	0.55 ± 0.09	−12.8
$R_{103}{}^{3'}T20D_{24}$	0.59 ± 0.11	1.26 ± 0.04	0.31 ± 0.03	−13.2

[a] Samples were equilibrated for 10 min at 30 °C in standard helicase buffer before analysis with a filter-binding assay as described previously (*7*). F_{max} is the maximal fraction of ^{32}P-labeled substrate retained on the nitrocellulose membrane, K_d is the dissociation constant, and n is the number of hexamers bound per substrate molecule.

Rho before addition of the ATP/Mg^{2+}/poly(rC) initiation mix (Figure 4D). Thus, the effect of 3′-ssDNA tails on the helicase reaction is not related to the kinetics of formation or strength of the initial Rho−substrate complex but rather stems from interference with a later step along the reaction pathway (most likely, the maturation into a functional complex; see Discussion). Note that the data also confirm that productive Rho association with RNA−DNA substrates is not adequately predicted by equilibrium binding measurements (*7*).

To determine which features of the $R_{103}{}^{3'Tn}D_{24}$ substrates are responsible for the decrease in reaction amplitude (Figure 4C), we changed the nature of the molecular appendage to the DNA strand. As shown in Figure 4E, reaction profiles were almost identical with substrates bearing a $d(T)_{10}$ or

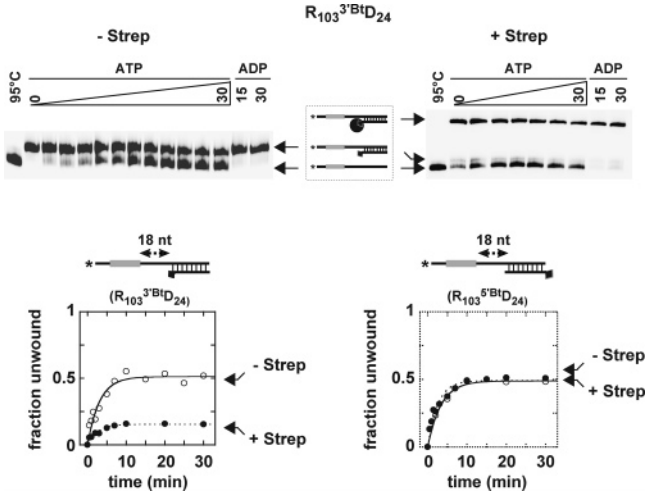

FIGURE 5: Influence of a biotin−streptavidin complex linked to the DNA strand of the $R_{103}D_{24}$ substrate on the Rho helicase. Reactions were performed under standard single-cycle conditions with the following modifications: the ^{32}P-labeled strand is the R_{103} transcript shown in Figure 4A; in appropriate samples, streptavidin (300 nM, final concentration) was incubated with the RNA−DNA construct containing a biotin moiety linked covalently to one end of the DNA strand ($R_{103}{}^{5'Bt}D_{24}$ or $R_{103}{}^{3'Bt}D_{24}$ substrate) for 10 min at 37 °C before addition of the Rho hexamers; the ATP/Mg^{2+} initiation mixture also contained an excess of biotin (3 μM, final concentration) to trap free streptavidin. Representative gels (10% polyacylamide; 0.3% SDS) showing unwinding of the biotinylated $R_{103}{}^{3'Bt}D_{24}$ substrate bound (+Strep) or not (−Strep) to streptavidin. Incubation times, in minutes, are indicated above gel lanes. The biotin and streptavidin moieties are depicted schematically by a black diamond and circle, respectively. The graphs show how the position of biotin coupling to the DNA strand affects the amount of substrate unwound during a single cycle of Rho helicase reaction. Data fits to an equation describing pseudo-first-order kinetics yield reaction amplitudes and rates of, respectively, ~0.5 and ~0.3 min^{-1} except for the $R_{103}{}^{3'Bt}D_{24}$−Strep complex (left graph) for which $A = 0.16 \pm 0.01$ and $k_{obs} = (0.36 \pm 0.05)$ min^{-1}.

$d(A)_{10}$ extension, thereby suggesting that the identity of the residues composing the 3′-ssDNA tail is unimportant ($d(C)_n$ and $d(G)_n$ tails were not probed because of their likelihood to perturb Rho binding to the substrate either directly or through interactions with the *aRut* sequence). A biotin−streptavidin complex in place of the 3′-ssDNA tail also significantly reduced the reaction amplitude (Figure 5, left graph). Notably, the same biotin−streptavidin complex had no effect on the helicase reaction when linked to the 5′-end rather than to the 3′-end of the DNA strand (Figure 5, right graph). The fact that the position but not the nature of the molecular appendage modulates the efficiency of RNA−DNA unwinding (Figures 4B,E and 5) pinpoints to steric hindrance as the source of the inhibition.

When combined together, the results presented in Figures 3−5 indicate that the effect induced by a 3′-ssDNA tail (or biotin−streptavidin extension) on the Rho helicase is not ubiquitous but context-dependent. The data also demonstrate the potential for functional interdependence between molecular appendages (such as the 5′-ssRNA and 3′-ssDNA tails) or adjuncts (such as streptavidin) to the NA substrate, a feature that may have important implications for biological regulation of the Rho enzyme. On the other hand and regardless of the reaction efficiency, the fact that a DNA strand bearing a biotin−streptavidin complex at its 3′-end can be removed by Rho (Figure 5) supports a steric exclusion mechanism for helicase action. This is because streptavidin

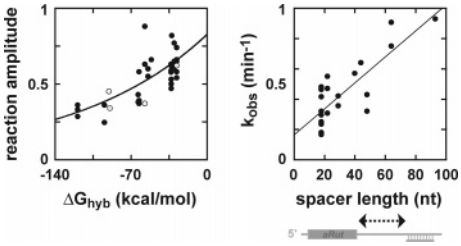

FIGURE 6: Influence of the RNA−DNA hybrid stability and distance between the *aRut* and hybrid regions on Rho helicase activity. Reactions were performed under standard single-turnover conditions with 22 distinct *aRut*-containing substrates (this work; ref *7*; C. Walmacq and M. Boudvillain, unpublished results). All the substrates contained a single and fully paired DNA strand hybridized at least 18 nt downstream from the 3′-end of an *aRut* site. However, the length of the transcript (103−214 nt) as well as the position and length (22−80 bp) of the RNA−DNA helix varied significantly. The curve on the left graph results from data fitting to the equation: $A = A_0 \times P^{(-\Delta Ghyb)}$, where A is the reaction amplitude, A_0 is the initial fraction of productive Rho−substrate complexes, P is the enzyme processivity, and ΔG_{hyb} is the energy of RNA−DNA hybrid formation (in kcal/mol). Open circles correspond to the fractions of oligonucleotides that are displaced from the $R_{157}D_{22a}D_{42a}$ and $R_{157}D_{42b}D_{22b}$ substrates in a single helicase turnover (see Figure 2B,C). For the trailing D_{42a} and D_{22b} strands, reaction amplitudes were plotted against ΔG_{hyb} values corresponding to the full 64 bp-long RNA−DNA hybrid regions.

is too large (~54 Å in diameter) to traverse the 20−35 Å-wide Rho central channel (*21*). Importantly, this conclusion holds true whether the biotin−streptavidin complex remains unaffected by RNA−DNA unwinding or whether Rho first dissociates streptavidin from the biotinylated D_{24} strand (in this case, the steric exclusion mechanism applies to Rho-induced disruption of the biotin−streptavidin complex).

Multiple Substrate Features Affect the Rho Helicase Reaction. We have now identified several structural parameters that can modulate the efficiency of unwinding of *aRut*-containing substrates by the Rho helicase: the length of the RNA−DNA helix and the distance between the *aRut* and hybrid regions (*7*) as well as the presence of a bulky appendage to the 3′-end of the DNA strand (see above). To determine whether other substrate feature(s) may influence Rho action, we have collected helicase reaction parameters for multiple *aRut*-containing RNA−DNA constructs. To facilitate the comparison, constructs wherein the RNA−DNA and *aRut* regions were too close (<18 nt) or those that contained DNA appendages or multiple RNA−DNA helices (such as $R_{115}D_{65}R_{43}$ or $R_{103}{}^{3'T20}D_{24}$ substrates) were excluded from the analysis. The reaction amplitudes and rates were obtained under standard single-run conditions (see Materials and Methods) for 22 distinct substrates. Scatterplots were then generated to detect potential covariances between reaction parameters and quantifiable substrate features (length, stability of the RNA−DNA helix, and so on). Only two such covariances could be inferred from this analysis: a 'processivity-like' dependence of reaction amplitude on hybrid stability ($R^2 = 0.49$, $p < 10^{-4}$; Figure 6, left graph) or length ($R^2 = 0.47$, $p < 10^{-4}$; data not shown) and, more surprisingly, a positive linear correlation between k_{obs} and the distance between the *aRut* and RNA−DNA hybrid regions ($R^2 = 0.67$, $p < 10^{-4}$; Figure 6, right graph). Despite good statistical significances ($p < 10^{-4}$), these relationships failed to explain substantial amounts of the variances in the

dependent variables (30 and 50% for reaction rates and amplitudes, respectively). This is illustrated by the residual dispersion of the data points around the curve fits (Figure 6) and suggests that other, as yet unrecognized, features of the substrates also control in part the efficiency of the Rho helicase.

DISCUSSION

A Steric Exclusion Mechanism for the Rho Helicase. Previous biochemical work has established that the Rho hexamer encircles its transcript substrate (*22*, *24*, *26*), a topological feature that is compatible with the various strand-exclusion models proposed for ring-shaped helicases (*3*). In addition, we now show that Rho−RNA contacts are important for the transduction of Rho helicase action and/or stability of the transient Rho−substrate complexes. Indeed, the presence of a nick in the RNA strand precludes unwinding of a reporter RNA−DNA helix located downstream from the nick (Figure 1). This effect is comparable to the inhibition of prototypical hexameric DNA helicases by a nick in the 'translocating' (loading) DNA strand (*32*−*34*). Thus, for the two types of enzymes, one of the NA strands is involved in critical interactions during both the loading and translocation steps. On the other hand, Rho-directed unwinding of RNA−DNA substrates was not affected by nicks in the 'nontranslocating' (displaced) DNA strand (Figure 2 and data not shown). Although comparable results were obtained with the replicative Mcm helicase from *Methanobacterium thermoautotrophicus* (*mt*Mcm), a nick in the displaced DNA strand inhibited unwinding of downstream DNA by the DnaB (from *Thermus aquaticus*) and eukaryotic Mcm counterparts (*32*, *34*). Thus, Rho also exhibits reactivity features distinct from those of model hexameric DNA helicases (note that we now know that the *mt*Mcm helicase assembles into a double-ring structure and probably utilizes a distinct mechanism; ref *48*). At the same time, the path of the RNA strand within the Rho hexamer (*22*, *24*, *26*), Rho asymmetric interaction with the two strands of an RNA−DNA hybrid (this work), as well as the enzyme capability to displace heterologous roadblocks such as NA oligonucleotides, a DNA strand protected by a bulky biotin−streptavidin 'bumper' (see results and Figure 5), or large nucleoprotein complexes (the biological TEC target; ref *2*; M. Boudvillain and A. R. Rahmouni, unpublished results), all are characteristics congruous with a strand-exclusion mechanism (*3*). Thus, both Rho and hexameric DNA helicases appear to rely on the same general mechanism of steric exclusion. This might have been imposed simply by a similar quaternary organization and/or may be due to cryptic elements of selective pressure common to the transcription termination and replication processes.

Mechanistic Differences between Rho and Hexameric DNA Helicases. All ring-shaped helicases may progress along their loading NA strand by pulling it actively into their central channel (*1*, *3*, *49*). At the same time, specimens such as DnaB or the eukaryotic Mcm use the ssDNA tail fronting the complementary strand (or another physical protuberance such as a biotin−streptavidin complex) as a molecular fulcrum to effect strand separation. In the absence of such a molecular appendage, both strands remain associated and are engulfed together within the helicase ring (translocation without associated unwinding activity; refs *32*−*34* and *50*). Although a protruding appendage to the DNA 3′-end may also favor Rho helicase activity in some cases (see Results and Figure 3B), the enzyme can efficiently dissociate DNA strands fully paired to the transcript substrate (*5*, *7*, *8*, *42*). At present, the structural origins for this difference in unwinding efficiency remain obscure, especially if one assumes a commonality of mechanism between Rho and hexameric DNA helicases (see above) and considers the similar sizes (20−30 Å) of their ring interior holes (*3*, *21*). Among possible explanations is the fact that the functional Rho hexamer may have an interior hole significantly smaller than was reported for its 'notched' crystallographic isoform (*21*). Alternatively, NA helices with strong A-like characters such as the RNA and RNA−DNA targets of the Rho helicase may exhibit sufficiently large hydrodynamic diameters (up to 30% more than for B-DNA) for direct steric exclusion from the hexamer center hole.

In some instances, the presence of a ssDNA tail can also have a strong deleterious effect on the efficiency of substrate unwinding by the Rho helicase ($R_{103}{}^{3'Tn}D_{24}$ substrates; Figure 4). This inhibitory effect, which has never been observed with another ring-shaped helicase (activation of DnaB unwinding by a 3'-ssDNA arm is downgraded for arm's lengths over 25 nt, however; see ref *30*), is likely to have a steric origin. Indeed, in the $R_{103}{}^{3'Tn}D_{24}$ substrates, the putative C-rich loading site (encompassing the minimal *aRut* sequence) and the RNA−DNA helix are juxtaposed (Figure 4A) instead of being far apart from one another (as in the $R_{157}{}^{3'Tn}D_{24}$ substrates; Figure 3). Although this juxtaposition does not affect Rho loading onto the substrate (Figure 4D and Table 1) nor unwinding of the bare $R_{103}D_{24}$ helix (Figure 4B), the presence of a molecular appendage to the D_{24} strand may hinder the formation of a fully productive (or adequately processive) Rho−substrate complex (Figures 4C,E and 5). We note that shortening (to 10 nt) the single-stranded spacer between the *aRut* sequence and the RNA−DNA helix induces a similar reduction of the reaction amplitude without affecting the affinity of Rho for the substrate (*7*). This previous result could also be explained by interference of a sterically inappropriate element (i.e., the RNA−DNA helix being too close to the Rho loading site) with a productive isomerization of the Rho−substrate complex early on the reaction pathway (i.e., first step shown in Figure 7; see also below). Moreover, the nature of the interfering factors (short single-stranded spacer, ssDNA tail, or biotin−streptavidin complex) implies that such an activation step would require substantial spatial freedom and, hence, trigger significant conformational changes within the Rho−substrate complex. Consistent with this proposal, biochemical and structural data suggest a sequence of conformational rearrangements for formation of a productive Rho−transcript complex (*21*, *51*, *52*). In this mechanism, inactive open Rho conformers interact initially with the transcript *Rut* sequence through their primary binding sites. This interaction drives the transcript downstream section toward the hexamer center where RNA contacts to the Rho secondary binding site subsequently trigger ring closure and activate ATP hydrolysis. We note that, in the case of replicative helicases, similar multistep pathways have been proposed for formation of productive enzyme−substrate complexes (reviewed in refs *29*, *53*). Although the organization of the primary binding site (*20*, *21*) makes Rho unique in its initial recognition of specific

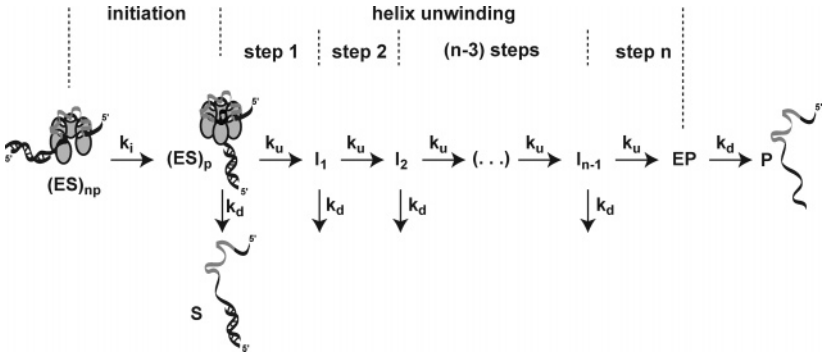

FIGURE 7: Schematic of the postulated Rho unwinding mechanism. The Rho−substrate complex (ES) is slowly activated (with $k_i \approx k_{obs}$) and then transformed into successive intermediate isoforms (I_1, I_2, ..., I_{n-1}) wherein the RNA−DNA hybrid is increasingly unwound (with $k_u \gg k_i$) until it collapses irreversibly (EP state). A fraction of Rho−substrate complexes dissociates at every step so that not all RNA−DNA hybrids can be unwound under single-turnover conditions. Although Rho translocation along the single-stranded spacer between the *aRut* and RNA−DNA regions is not formerly represented, it may also occur through discrete steps. In this respect, it should be stressed that none of the steps depicted in the figure represent actual elementary reactions (see ref *58*). Similarly, the molecular details of Rho activation (initiation step) may differ from the ones shown, and one or several reaction steps may be reversible.

single-stranded RNA targets (the *Rut* sites), replication auxiliary factors such as primase domains, either provided in trans (e.g., T4 gp61) or fused to the helicase domain (as for T7 gp4), may also help loading of replicative helicases in a comparable way (*27*, *53*). In summary, our results suggest that Rho, as other hexameric helicases, effects actual NA unwinding by a steric exclusion mechanism. However, even in the absence of a protruding appendage, the respective shapes and dimensions of the Rho channel and NA target (RNA or RNA−DNA helix) permit efficient exclusion of the displaced strand in most cases. Rho also slightly differs from its ring-shaped homologues by its specific mode of substrate recognition which, however, likely includes a similar multistep pathway towards the formation of a fully productive enzyme−substrate complex.

Formation of a Productive Rho−RNA Complex Is a Crucial Rate-Limiting Event. Single-turnover unwinding experiments can provide useful insights on the translocation mechanism and processivity of an helicase (*54*). Because every helicase molecule dissociating from the NA substrate is captured and inactivated by 'trap' molecules, the amplitude of a single-run reaction is directly related to the fraction of productive helicase−substrate complexes formed initially as well as to all the helicase release events that occur before irreversible separation of the NA strands (i.e., when too many bp have been open to leave a stable helix). We observed previously that the amplitudes of Rho helicase reactions tend to diminish when the length of the RNA−DNA hybrid is increased within *aRut*-containing substrates (*7*). Using classical analysis, we deduced that Rho unwinds RNA−DNA regions in a succession of moderately processive discrete steps, so that, on average, 60−80 hybrid bp are unwound before dissociation of the enzyme−substrate complex (*7*). Because the reaction kinetics were hardly sensitive to the hybrid length, the size of the elementary translocation steps could not be resolved kinetically. For the same reason, we also concluded that hybrid unwinding is rate-limited by a slow reaction event distinct from the unwinding steps (*7*). A simple mechanism that is compatible with these observations is depicted schematically in Figure 7. In this mechanism, the conversion of the Rho−substrate complex into an active isoform [$(ES)_p$] precedes a succession of fast unwinding steps until the RNA−DNA hybrid is completely disrupted. The fact that the overall process is kinetically controlled by a slow initiation step (which may, however, include helicase positioning in front of the RNA−DNA helix) is supported by experiments performed with the $R_{157}D_{22a}D_{42a}$, $R_{157}D_{42b}D_{22b}$, and $R_{157}D_{22a}D_{22b}$ substrates wherein both the leading and trailing DNA strands are released without delays and at the same rate (Figure 2 and data not shown). Interestingly, the rate of this kinetic-limiting step (as represented by k_{obs}) appears to depend, at least in part, on the position of the reporter RNA−DNA helix with respect to the *aRut* loading site (Figure 6). This positive correlation is consistent with the proposal formulated above whereby formation of a productive Rho−substrate complex involves large conformational rearrangements and therefore requires substantial spatial freedom. It follows from these observations that productive isomerization of the Rho−substrate complex, as schematically depicted in Figure 7 (initiation step), likely represents the rate-limiting step of our helicase reactions. We note that for all Rho helicase experiments reported to date (with substrates derived from the *Escherichia coli* trpt′, *λ*cro gene products or from *aRut*-containing transcripts; refs *5*−*8*, *42*, *43*, *55*, *56*) k_{obs} values are of comparable magnitude (when corrected for temperature differences), and reaction progress curves do not exhibit lag phases that would be indicative of kinetic control by events made of multiple repeated steps (such as helicase translocation and NA unwinding). Thus, a Rho helicase activity that is rate-limited by a slow initiation step may hold true for a broad range of experimental conditions. Formation of a Rho−RNA complex competent in ATPase activity appears to occur on a much faster time-scale ($k_{activation} > 180$ min^{-1} at 18 °C; ref *52*). This difference may be due to the utilization of an 'overpotent' RNA cofactor (poly(rC)) in the ATPase experiments (*52*). Alternatively, the Rho−RNA complex may need to undergo further rearrangement(s) before acquiring full mechanochemical competence (this latter initiation step(s) would then control kinetically the helicase reaction). Whether and how these observations may translate in vivo in the context of transcription termination remain a matter of speculation. However, it is noteworthy that kinetic control early on the reaction pathway would facilitate oversight by transcription auxiliary factors and/or shutoff of unwanted termination events before any harm is done to the working TEC.

Idiosyncratic Rho Helicase Responses to Substrate Composition. Before each elementary unwinding step, some Rho

hexamers dissociate from the substrate rather than reiterate unwinding (Figure 7), so that the longer the RNA−DNA helix, the smaller the fraction of hybrids that end up unwound under single-run conditions (*7*). In accord with this mechanism, Rho displaced the trailing D_{42a} oligonucleotide from the $R_{157}D_{22a}D_{42a}$ substrate in lower amounts than the leading D_{22a} strand (Figure 2B). Yet, with the other composite substrate ($R_{157}D_{42b}D_{22b}$), the two contiguous oligonucleotides were removed in comparable proportions (Figure 2B). To understand this discrepancy, one can use the wealth of experimental data that has now been collected with various *aRut*-containing substrates (this work; ref *7*; C. Walmacq, A. R. Rahmouni, and M. Boudvillain, unpublished results). As shown in Figure 6, there is a significant variability of the amplitude of the helicase reaction for a given hybrid stability (or size; data not shown). This variability alone could account for the differential results obtained with the composite $R_{157}D_{22a}D_{42a}$ and $R_{157}D_{42b}D_{22b}$ substrates. In effect, each oligonucleotide is released from these substrates in amounts (Figure 6, open circles) that lie well within the limits of the experimental data set.

Aside from standard error deviations, the variability of the reaction amplitude observed for a given hybrid size (or stability; Figure 6) could stem from idiosyncratic helicase responses to specific experimental features. For instance, poly(rC), which is used as a Rho trap in single-run helicase experiments, can boost the efficiency of the Rho helicase under particular conditions (*7*). Features more specific to the substrate are also known to affect Rho helicase action. This is notably the case of structural determinants such as the composition (RNA or RNA−DNA) of the reporter helix (*6*), its distance from the Rho loading site (*7*), or the global secondary and/or tertiary structure of the construct (*43*). The data obtained with the forked RNA−DNA constructs (Figures 3 and 4), which have not been included in the analysis of the reaction amplitude (Figure 6), now provide another compelling example of Rho idiosyncratic reactivity to the structure of the substrate. We note, however, that this property could significantly complicate the evaluation of Rho processivity as variations of the amplitude of the helicase reaction may not be linked merely to changes of the length of the reporter hybrid. Thus, even though our initial estimation of Rho processivity ($P = 0.985$/bp, which was obtained with an homogeneous set of substrates; see ref *7*) does not seem much affected by the greater heterogeneity of the expanded data set ($P = 0.987$/bp or 0.992 mol/kcal; Figure 6 and data not shown), Rho may in fact, depending on context, significantly deviate from such average behavior. Structural features of the Rho substrate may also affect the fraction of productive complex formed initially, as suggested by results with the $R_{103}{}^{3'Tn}D_{24}$ substrates (see above and Figure 4). Either way (modulation of the complex's productivity or processivity) offers an attractive mechanistic solution for regulation of Rho function through 'sensing' of the structure of the substrate. However, whether and which of these solutions is involved in vivo in the various modes of structural and factor-dependent modulation of Rho-dependent termination of transcription (*2*, *57*) await further analysis.

ACKNOWLEDGMENT

We gratefully acknowledge J. P. Richardson and P. H. von Hippel for the gift of materials, A. Schwartz for her technical assistance, as well as M. Kashlev, F. Boccard, and E. Delagoutte for helpful discussions.

REFERENCES

1. Richardson, J. P. (2003) Loading Rho to terminate transcription, *Cell 114*, 157−159.
2. Richardson, J. P. (2002) Rho-dependent termination and ATPases in transcript termination, *Biochim. Biophys. Acta 1577*, 251−260.
3. Patel, S. S., and Picha, K. M. (2000) Structure and function of hexameric helicases, *Annu. Rev. Biochem. 69*, 651−697.
4. Lowery-Goldhammer, C., and Richardson, J. P. (1974) An RNA-dependent nucleoside triphosphate phosphohydrolase (ATPase) associated with rho termination factor, *Proc. Natl. Acad. Sci. U.S.A. 71*, 2003−2007.
5. Brennan, C. A., Dombroski, A. J., and Platt, T. (1987) Transcription termination factor rho is an RNA-DNA helicase, *Cell 48*, 945−952.
6. Brennan, C. A., Steinmetz, E. J., Spear, P., and Platt, T. (1990) Specificity and efficiency of rho-factor helicase activity depends on magnesium concentration and energy coupling to NTP hydrolysis, *J. Biol. Chem. 265*, 5440−5447.
7. Walmacq, C., Rahmouni, A. R., and Boudvillain, M. (2004) Influence of substrate composition on the helicase activity of transcription termination factor Rho: reduced processivity of Rho hexamers during unwinding of RNA-DNA hybrid regions, *J. Mol. Biol. 342*, 403−420.
8. Walstrom, K. M., Dozono, J. M., Robic, S., and von Hippel, P. H. (1997) Kinetics of the RNA-DNA helicase activity of *Escherichia coli* transcription termination factor rho. 1. Characterization and analysis of the reaction, *Biochemistry 36*, 7980−7992.
9. Steinmetz, E. J., Brennan, C. A., and Platt, T. A (1990) Short intervening structure can block rho factor helicase action at a distance, *J. Biol. Chem. 265*, 18408−18413.
10. Zalatan, F., Galloway-Salvo, J., and Platt, T. (1993) Deletion analysis of the *Escherichia coli* rho-dependent transcription terminator trp t′, *J. Biol. Chem. 268*, 17051−17056.
11. Hart, C. M., and Roberts, J. W. (1994) Deletion analysis of the lambda tR1 termination region. Effect of sequences near the transcript release sites, and the minimum length of rho-dependent transcripts, *J. Mol. Biol. 237*, 255−265.
12. Chen, C. Y., Galluppi, G. R., and Richardson, J. P. (1986) Transcription termination at lambda tR1 is mediated by interaction of rho with specific single-stranded domains near the 3′ end of cro mRNA, *Cell 46*, 1023−1028.
13. Chen, C. Y., and Richardson, J. P. (1987) Sequence elements essential for rho-dependent transcription termination at lambda tR, *J. Biol. Chem. 262*, 11292−11299.
14. Hart, C. M., and Roberts, J. W. (1991) Rho-dependent transcription termination. Characterization of the requirement for cytidine in the nascent transcript, *J. Biol. Chem. 266*, 24140−24148.
15. Wang, Y., and von Hippel, P. H. (1993) *Escherichia coli* transcription termination factor rho. II. Binding of oligonucleotide cofactors, *J Biol Chem. 268*, 13947−13955.
16. Wang, Y., and von Hippel, P. H. (1993) *Escherichia coli* transcription termination factor rho. I. ATPase activation by oligonucleotide cofactors, *J. Biol. Chem. 268*, 13940−13946.
17. Zalatan, F., and Platt, T. (1992) Effects of decreased cytosine content on rho interaction with the rho-dependent terminator trp t′ in *Escherichia coli*, *J. Biol. Chem. 267*, 19082−19088.
18. Alifano, P., Rivellini, F., Limauro, D., Bruni, C. B., and Carlomagno, M. S. (1991) A consensus motif common to all Rho-dependent prokaryotic transcription terminators, *Cell 64*, 553−563.
19. Guerin, M., Robichon, N., Geiselmann, J., and Rahmouni, A. R. (1998) A simple polypyrimidine repeat acts as an artificial Rho-dependent terminator in vivo and in vitro, *Nucleic Acids Res. 26*, 4895−4900.
20. Bogden, C. E., Fass, D., Bergman, N., Nichols, M. D., and Berger, J. M. (1999) The structural basis for terminator recognition by the Rho transcription termination factor, *Mol. Cell 3*, 487−493.
21. Skordalakes, E., and Berger, J. M. (2003) Structure of the rho transcription terminator. Mechanism of mRNA recognition and helicase loading, *Cell 114*, 135−146.
22. Burgess, B. R., and Richardson, J. P. (2001) RNA passes through the hole of the protein hexamer in the complex with the *Escherichia coli* Rho factor, *J. Biol. Chem. 276*, 4182−4189.

23. Gogol, E. P., Seifried, S. E., and von Hippel, P. H. (1991) Structure and assembly of the *Escherichia coli* transcription termination factor rho and its interaction with RNA. I. Cryoelectron microscopic studies, *J. Mol. Biol. 221*, 1127−1138.
24. Wei, R. R., and Richardson, J. P. (2001) Identification of an RNA-binding site in the ATP binding domain of *Escherichia coli* Rho by H2O2/Fe-EDTA cleavage protection studies, *J. Biol. Chem. 276*, 28380−28387.
25. Richardson, J. P. (1982) Activation of rho protein ATPase requires simultaneous interaction at two kinds of nucleic acid-binding sites, *J. Biol. Chem. 257*, 5760−5766.
26. Wei, R. R., and Richardson, J. P. (2001) Mutational changes of conserved residues in the Q-loop region of transcription factor Rho greatly reduce secondary site RNA-binding, *J. Mol. Biol. 314*, 1007−1015.
27. Davey, M. J., and O'Donnell, M. (2003) Replicative helicase loaders: ring breakers and ring makers, *Curr. Biol. 13*, R594−596.
28. Hickman, A. B., and Dyda, F. (2005) Binding and unwinding: SF3 viral helicases, *Curr. Opin. Struct. Biol. 15*, 77−85.
29. Sclafani, R. A., Fletcher, R. J., and Chen, X. S. (2004) Two heads are better than one: regulation of DNA replication by hexameric helicases, *Genes Dev. 18*, 2039−2045.
30. Galletto, R., Jezewska, M. J., and Bujalowski, W. (2004) Unzipping mechanism of the double-stranded DNA unwinding by a hexameric helicase: the effect of the 3′ arm and the stability of the dsDNA on the unwinding activity of the *Escherichia coli* DnaB helicase, *J. Mol. Biol. 343*, 101−114.
31. Hacker, K. J., and Johnson, K. A. (1997) A hexameric helicase encircles one DNA strand and excludes the other during DNA unwinding, *Biochemistry 36*, 14080−14087.
32. Kaplan, D. L. (2000) The 3′-tail of a forked-duplex sterically determines whether one or two DNA strands pass through the central channel of a replication-fork helicase, *J. Mol. Biol. 301*, 285−299.
33. Kaplan, D. L., Davey, M. J., and O'Donnell, M. (2003) Mcm4,6,7 uses a "pump in ring" mechanism to unwind DNA by steric exclusion and actively translocate along a duplex, *J. Biol. Chem. 278*, 49171−49182.
34. Shin, J. H., Jiang, Y., Grabowski, B., Hurwitz, J., and Kelman, Z. (2003) Substrate requirements for duplex DNA translocation by the eukaryal and archaeal minichromosome maintenance helicases, *J. Biol. Chem. 278*, 49053−49062.
35. Kaplan, D. L., and Steitz, T. A. (1999) DnaB from *Thermus aquaticus* unwinds forked duplex DNA with an asymmetric tail length dependence, *J. Biol. Chem. 274*, 6889−6897.
36. Ahnert, P., and Patel, S. S. (1997) Asymmetric interactions of hexameric bacteriophage T7 DNA helicase with the 5′- and 3′-tails of the forked DNA substrate, *J. Biol. Chem. 272*, 32267−32273.
37. Kaplan, D. L., and O'Donnell, M. (2003) Rho factor: transcription termination in four steps, *Curr. Biol. 13*, R714−716.
38. Nowatzke, W., Richardson, L., and Richardson, J. P. (1996) Purification of transcription termination factor Rho from *Escherichia coli* and *Micrococcus luteus*, *Methods Enzymol. 274*, 353−363.
39. Schwartz, A., Rahmouni, A. R., and Boudvillain, M. (2003) The functional anatomy of an intrinsic transcription terminator, *EMBO J. 22*, 3385−3394.
40. Zuker, M. (2003) Mfold web server for nucleic acid folding and hybridization prediction, *Nucleic Acids Res. 31*, 3406−3415.
41. Sugimoto, N., Nakano, S., Katoh, A., Nakamura, H., Ohmichi, T., Yoneyama, M., and Sasaki, M. (1995) Thermodynamic parameters to predict the Stability of RNA/DNA hybrid duplexes, *Biochemistry 34*, 11211−11216.
42. Walstrom, K. M., Dozono, J. M., and von Hippel, P. H. (1997) Kinetics of the RNA-DNA helicase activity of *Escherichia coli* transcription termination factor rho. 2. Processivity, ATP consumption, and RNA binding, *Biochemistry 36*, 7993−8004.
43. Walstrom, K. M., Dozono, J. M., and von Hippel, P. H. (1998) Effects of reaction conditions on RNA secondary structure and on the helicase activity of *Escherichia coli* transcription termination factor Rho, *J. Mol. Biol. 279*, 713−726.
44. Lane, M. J., Paner, T., Kashin, I., Faldasz, B. D., Li, B., Gallo, F. J., and Benight, A. S. (1997) The thermodynamic advantage of DNA oligonucleotide 'stacking hybridization' reactions: energetics of a DNA nick, *Nucleic Acids Res. 25*, 611−617.
45. Bianco, P. R., and Kowalczykowski, S. C. (2000) Translocation step size and mechanism of the RecBC DNA helicase, *Nature 405*, 368−372.
46. Jankowsky, E., Gross, C. H., Shuman, S., and Pyle, A. M. (2000) The DExH protein NPH-II is a processive and directional motor for unwinding RNA, *Nature 27*, 447−451.
47. Cleveland, W. S. (1979) Robust locally weighted regression and smoothing scatter plots, *J. Am. Stat. Assoc. 74*, 829−836.
48. Gomez-Llorente, Y., Fletcher, R. J., Chen, X. S., Carazo, J. M., and San Martin, C. (2005) Polymorphism and double hexamer structure in the archaeal minichromosome maintenance (MCM) helicase from *Methanobacterium thermoautotrophicum*, *J. Biol. Chem. 280*, 40909−40915.
49. Ogura, T., and Wilkinson, A. J. (2001) AAA+ superfamily ATPases: common structure−diverse function, *Genes Cells 6*, 575−597.
50. Kaplan, D. L., and O'Donnell, M. (2002) DnaB drives DNA branch migration and dislodges proteins while encircling two DNA strands, *Mol. Cell 10*, 647−657.
51. Jeong, Y. J., Kim, D. E., and Patel, S. S. (2004) Nucleotide binding induces conformational changes in *Escherichia coli* transcription termination factor Rho, *J. Biol. Chem. 279*, 18370−18376.
52. Kim, D. E., and Patel, S. S. (2001) The kinetic pathway of RNA binding to the *Escherichia coli* transcription termination factor Rho, *J. Biol. Chem. 276*, 13902−13910.
53. Delagoutte, E., and von Hippel, P. H. (2003) Helicase mechanisms and the coupling of helicases within macromolecular machines. Part II: Integration of helicases into cellular processes, *Q. Rev. Biophys. 36*, 1−69.
54. Lucius, A. L., Maluf, N. K., Fischer, C. J., and Lohman, T. M. (2003) General methods for analysis of sequential "n-step" kinetic mechanisms: application to single turnover kinetics of helicase-catalyzed DNA unwinding, *Biophys. J. 85*, 2224−2239.
55. Brennan, C. A., and Platt, T. (1991) Mutations in an RNP1 consensus sequence of Rho protein reduce RNA binding affinity but facilitate helicase turnover, *J. Biol. Chem. 266*, 17296−17305.
56. Burgess, B. R., and Richardson, J. P. (2001) Transcription factor Rho does not require a free end to act as an RNA-DNA helicase on an RNA, *J. Biol. Chem. 276*, 17106−17110.
57. Greive, S. J., and von Hippel, P. H. (2005) Thinking quantitatively about transcriptional regulation, *Nat. Rev. Mol. Cell Biol. 6*, 221−232.
58. Galletto, R., Jezewska, M. J., and Bujalowski, W. (2004) Unzipping mechanism of the double-stranded DNA unwinding by a hexameric helicase: quantitative analysis of the rate of the dsDNA unwinding, processivity and kinetic step-size of the *Escherichia coli* DnaB helicase using rapid quench-flow method, *J. Mol. Biol. 343*, 83−99.

BI0600648